EMADDC: high volume, high quality, ~~quickly available~~ and ~~high volume~~ timely wind and temperature observations from aircraft ~~using the~~ surveillance data (Mode-S EHS~~infrastructure~~)

Siebren de Haan[1], Paul de Jong[1,*], Michal Koutek[1,*], Jan Sondij[1], and Lukas Strauss[2]

[1]KNMI, De Bilt, The Netherlands
[2]Austro Control Digital Services, Vienna, Austria
[*]These authors contributed equally to this work.

Correspondence: Siebren de Haan (Siebren.de.Haan@knmi.nl)

Abstract. ~~Temperature and wind~~ Wind and temperature observations from aircraft are ~~regarded~~ of major importance for aviation meteorology and numerical weather prediction (NWP). The European Meteorological Aircraft Derived Data Center (EMADDC) system processes aircraft surveillance data received from air traffic control (ATC) and ~~converts it into~~ other partners and converts them into upper air observations of wind and temperature. Only so-called Mode-S Enhanced Surveillance data can be used, because ~~this data contains~~ these data contain the air vector and ground vector of the aircraft, from which a wind vector can be inferred. ~~To acquire~~ Temperature is derived from true airspeed and Mach number measurements. To produce high quality observations, the data ~~is~~ are processed in three steps: pre-processing, processing, and post-processing. The pre-processing is needed to obtain high-quality information and to calculate several correction values ~~such as temperature corrections and heading corrections~~for correcting temperature observations and heading values. Processing converts the aircraft data into meteorological information and finally post-processing guarantees that only high-quality information is made available. ~~The quality of the~~

The EMADDC system processes around 75×10^6 surveillance observations per day and produces over 55×10^6 observations of quality controlled wind observations and 32×10^6 temperature observations in the European airspace per day. The average age of the observation is around 5 to 10 minutes, depending on the method of data delivery (files via ftp or streaming constantly).

The quality of the observations produced is verified by comparing these observation to other upper air wind and temperature observations from radiosondes and Aircraft Meteorological Data Relay (AMDAR) and comparing them with NWP data. The quality of wind observations is almost identical to AMDAR, the quality of the temperature of EMADDC observations is lower but with bias is around zero, while AMDAR exhibits a positive bias of 0.5K.

This paper presents the EMADDC (R2.2) system, operational since 2019.

1 Introduction

For normal, and safe, operation, aircraft are equipped with sensors to measure ~~for example its height ,~~ height and velocity with respect to the surrounding air. These sensors can be exploited to observe wind and temperature at the aircraft's location ~~(Painting, 2003)~~(WMO, 2023). For many years, aircraft observations ~~form the backbone~~ are an essential component of the global observing system which is used as input for numerical weather prediction models during assimilation (Cardinali et al., 2003; James et al., 2020; Li, 2021; Strajnar et al., 2015; de Haan, 2013). For almost 30 years, aircraft measurements have been collected using the Aircraft Meteorological Data Relay (AMDAR), where meteorological information is automatically sent to national weather services using either satellites or ground stations (Ingleby et al., 2020; Barwell and Lorenc, 1985; Cardinali et al., 2003; James et al., 2020; Lange and Janjić, 2016; Li, 2021; Petersen, 2016; Zhu et al., 2015; Benjamin et al., 2010). Dedicated aircraft ~~were~~ are equipped with software to collect the relevant information from the onboard computer systems. Observations are collected with specified observation strategies to optimize coverage with respect to data transmission costs. ~~The~~ Over the last decade, a different manner of collecting meteorological information was developed utilizing the operational infrastructure for aircraft safety in Europe, starting in the area of Germany, Belgium and The Netherlands. The infrastructure used by the European Air Traffic Control (ATC) is based on Mode-selective (Mode-S) radars which (selectively) interrogate all aircraft in view of the radar on information on the ~~intended heading,~~ heading, true airspeed etc., to guide aircraft through its airspace (de Haan, 2011). Although in the whole European airspace Mode-S radars are used for ATC, not all received information can be used to refer to meteorological information, only Mode-S ~~enhanced surveillance~~ Enhanced Surveillance (Mode-S EHS) radars can interrogate the necessary ~~BDS5.0 and BDS6.0~~ Broadcast Dependent Surveillance (BDS) 5.0 and 6.0 registers. Fortunately, ~~the most of~~ most Mode-S radars in Europe have EHS capabilities. The observation frequency is determined by the interrogation frequency of the Mode-S radar. To extract meteorological information from the received BDS5.0 and BDS6.0 registers, processing and corrections are needed ~~(de Haan, 2011). Due to the COVID19-pandemic,~~ (de Haan, 2011; Stone and Pearce, 2016) .

In light of the COVID-19 pandemic, there was a significant reduction in the number of flights ~~dramatically decreased (Dube, 2023) and with it~~ (Dube, 2023), which in turn impacted the availability of temperature and wind observations ~~performed by dedicated aircraft collected through~~ collected through the Aircraft Meteorological Data Relay (AMDAR). ~~However, whilst some airlines were still flying (e.g. cargo flights)~~Nevertheless, as certain airlines continued to operate, such as cargo flights, the European Meteorological Aircraft Derived Data Center (EMADDC) was still producing valuable observations, exploiting the ATC information received for surveillance of all flying aircraft. These observations were used by ~~ECMWF-IFS (Ingleby et al., 2021)~~ ECMWF (Ingleby et al., 2021) to address the gap resulting from the lack of AMDAR observations.

This paper describes the current state of the art ~~implemented~~ processing and correction methodology ~~as implemented for the~~ (R2.2) as implemented at EMADDC.

2 EMADDC Data Collection

~~Functional data flow in EMADDC, needed to derive wind vector and temperature observations.~~

Secondary Surveillance Radar (SSR) is a two-way system where an ATC radar interrogates an aircraft requesting specific parameters. In Europe, all large aircraft (with ~~so-called~~ minimum take-off weight larger than 5700 kg) are required to broadcast Mode-S Elementary Surveillance (ELS) and Enhanced Surveillance (EHS) (European Commission, 2011). ~~The EMADDC processing system derives~~ EMADDC exploits these to derive wind speed, wind direction and temperature observations from surveillance data requested from aircraft for ATC purposes. Where Elementary Surveillance only broadcasts altitude and identity, Enhanced Surveillance complements these basic parameters with data of the aircraft state, such as roll angle, air speed and Mach number. These additional parameters are requested in groups as a BDS request. To derive wind and temperature, EMADDC requires both BDS5.0 and BDS6.0 to be interrogated and broadcasted.

Additional to these mandatory BDS registers ~~,~~ BDS5.0 and BDS6.0, the BDS4.4 ~~,~~ register known as the Meteorological Routine Air Report or MRAR can be also interrogated~~, which will request the~~ . This register contains observed temperature, wind, static pressure and humidity (where available). However, this register is not mandatory and only ~~few (less~~ fewer than 5% ~~)~~ of aircraft respond to such interrogation requests (Strajnar, 2012) ~~. This is also the reason only~~ and few countries actively interrogate this register~~to reduce over-interrogation.~~

2.1 ~~Mode-S EHS Interrogation~~

.

~~ATC radar sends an interrogation or~~

2.1 Mode-S EHS Interrogation

ATC radar initiates a request to an aircraft ~~requesting a response for certain BDS registers. The aircraft in turn will respond, if it is equipped, and broadcasts~~ for specific BDS data registers. If the aircraft is appropriately equipped, it will respond by broadcasting the requested register ~~. It should be noted that not all Mode-S equipped radars are able to interrogate all the required registers to derive temperature and wind or do not interrogate all BDS registers during each radar rotation. Each country~~ information. Each radar employs a distinct interrogation scheme that outlines the frequency of requests and the specific registers to be queried. Different countries or Air Traffic Service Air Navigation Service ~~Provider (ATS ANSP) may interrogate aircraft differently and at various times and~~ Providers (ATS ANSPs) may utilize varying interrogation protocols, including different frequencies and rates. The response sent by the aircraft is received by ATC radar but can also be received through a commercially available local ~~Mode-S/ADS-B~~ receiver, as data is not encrypted. Unfortunately, it is more difficult to decode data received by these ~~reseceivers~~ receivers as the type of register is not contained in the transmission and hence fuzzy logic or other techniques ~~shall be~~ are applied to decode the type transmitted properly ~~.~~ (de Haan, 2011; Stone and Pearce, 2016). An in-house developed c-code software performs this task (similar to the python library developed by Sun (2021)).

2.2 Aircraft Dependent Surveillance-Broadcast

Aircraft Dependent Surveillance-Broadcast, or ADS-B, as its name suggests, allows an aircraft to broadcast aircraft state data using the transponder. Data is autonomously broadcast about every 0.5 seconds and contains the aircraft's onboard sensed position (through GPS and inertial systems) which is often more accurate than radar derived position from ATC. This data is available to ATC but ~~also~~ can also be displayed on the Navigation Display of newer aircraft for situational awareness. ADS-B does not broadcast wind and temperature, nor does it broadcast all required parameters to derive wind and temperature, ~~allthough~~ although the difference between GNSS height and pressure altitude is transmitted frequently and could be used in data assimilation ~~(?). Note that the content of messages is may differ for each aircraft.~~ (Stone and Kitchen, 2015).

2.3 ~~Aircraft Dependent Surveillance-Contract~~Data Handling

~~Aircraft Dependent Surveillance-Contract (ADS-C) differs from ADS-B as it reports to a single ground station in control of the contract. The ground station controls the content of the data to be transmitted back. The content can contain observed wind and temperature and even the aircraft trajectory. The update rate is typically lower than that of ADS-B.~~

3 ~~Data Handling~~

~~EMADDC receives aircraft data directly from~~ As outlined in the previous sections, EMADDC receives data in two ways: 1) aircraft data are collected by ATC, or ~~by collection~~ 2) aircraft data are collected using a local ~~Mode-S/~~ADS-B~~receiver. The first method~~ /Mode-S receiver. In both cases data is then forwarded to EMADDC through an FTP file transfer. New methods are currently being developed to enhance real-time data transfer, including NewPENS (the pan-European network for real-time exchange of air traffic control data).

Data collected by ATC delivers data of high quality as the content is properly decoded since the content of each transmission is known ~~. ATC also supplies~~ to the interrogator. Contrary for local receivers, the content of a received register is unknown and logic is required to verify that a register is correctly decoded. Data received from ATC radars or trackers is also processed and has quality control and filtering ~~on the data supplied.~~ applied.

Data can be of ASTERIX CAT48 format, which is mono-radar data, or CAT62 data from a radar tracker combining multiple radars. This latter data uses filtering to sample all radar plots to a typical 4 second interval. The content of ~~these formats~~ the formats CAT48 and CAT62 is similar but the typical resolution of the Mach number in CAT62 is ~~lower and hence~~ 0.008 (0.004 for CAT48), and as a consequence the derived temperature are of lower quality ~~. For this, multiple solutions are available where the first uses a different parameter field to supply the Mach number in higher resolution.~~ (see Section 6). EMADDC is working with EUROCONTROL ~~MUAC~~ Maastricht Upper Area Control Centre (MUAC) to develop a solution ~~. Another option is to derive~~ that provides the Mach number ~~from the indicated airspeed (Strauss, 2017).~~ with a resolution of 0.004 and share this solution with other ATC providers.

An advantage of radar or tracker data is that ~~BDS messages~~ the individual BDS messages corresponding to a single revolution of the radar are combined into a single "observation" message. ~~For~~ For ATC radar or tracker data, the position is determined by ATC radar~~while~~ . In contrast, for data received ~~by a local receiver~~from local receivers, the position is decoded from the Compact Position Report (CPR) format~~which is part of~~ , which is included in the ADS-B message ~~, and the timestamp is supplied by the receiver and not~~ (and hence not present in radar/tracker data as this data is not available in ASTERIX CAT48 or CAT62 data). The timestamp is not generated by the aircraft~~and EMADDC system needs to combine the different BDS registers~~ ; instead, it is created by the radar or receiver at the time of reception. Local receivers utilize either a GPS antenna or a time server for time synchronization. Furthermore, the EMADDC system must combine the various BDS registers to derive observations, as previously outlined.

The techniques ~~applied~~ utilized by EMADDC are ~~delivering enormous amounts~~ generating significant volumes of high-quality data from Mode-S EHS data. ~~However, several~~ It is essential to implement various quality control checks ~~need to be applied to capture observation imperfections.~~ to identify and address any observation discrepancies and assure that generated observations are of high quality.

3 Aircraft ~~measurement methodology~~Measurement Methodology

A modern aircraft is equipped with sensors that can measure static pressure~~or pressure altitude~~, Mach number, temperature, position and heading, and Geometric altitude. This section ~~conains~~ contains a brief description of measurements of pressure, Mach and temperature. The information flow is depicted in Figure 1.

3.1 Mach ~~number~~ Number and ~~static~~ Static and ~~total pressure~~Total Pressure

A crucial measurement in any aircraft is the measurement of the air speed, which can be obtained from the combination of a pitot-tube measurement and a temperature measurement. The pitot-tube measures the static pressure p_s and the total pressure p_t (Ruijgrok, 1990). Both pressure observations suffer from inaccuracies related to for example a (small) angle between the flow and the probe (Rodi and Leon, 2012). The Mach number is the true airspeed of the aircraft relative to the speed of sound. ~~It is measured (almost directly) by a pitot-probe.~~ Let $q_t = p_t - p_s$ be the dynamic pressure, which is more accurately measured because the first order error of p_t and p_s are canceled. Then, (Ruijgrok, 1990),

$$M = \sqrt{5\left(1+\frac{q_t}{p_s}\right)^{2/7}-1}\sqrt{\frac{2}{\gamma-1}\left(1+\frac{q_t}{p_s}\right)^{\frac{\gamma-1}{\gamma}}-1}, \tag{1}$$

where $\gamma = c_p/c_v$ is the ratio of specific heats. Note that the dependence of ~~M~~ M on the (inaccurate) p_s remains.

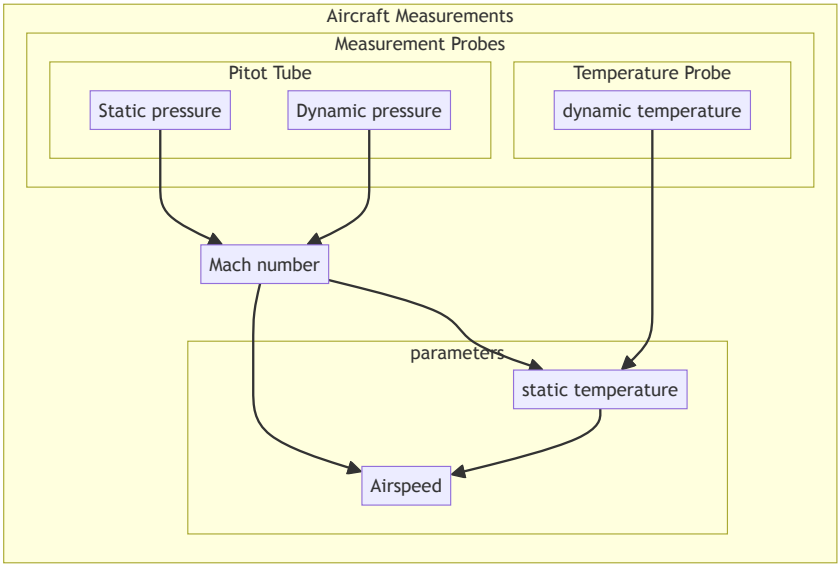

Figure 1. Information flow of aircraft measurements.

3.2 Temperature and True Airspeed

The temperature is measured with a temperature probe (Ruijgrok, 1990). The measured total temperature T_t needs to be corrected to obtain the ~~(ambient)~~ temperature T,

$$T_t = T_t \left(1 + \lambda \frac{(\gamma - 1)}{2} M^2\right)^{-1} \tag{2}$$

The true airspeed A can now be determined neglecting the effect of humidity,

$$A = M\sqrt{\gamma R_d T}, \tag{3}$$

where R_d is the universal gas constant of dry air.

4 EMADDC Measurement Methodology

Temperature and wind information is not directly available in Mode-S EHS downlinked information. The wind vector needs to be computed and the temperature needs to be derived, see Figure 2.

4.1 Downlinked ~~parameters~~Parameters

The (most relevant) parameters obtained through interrogation of Mode-S EHS radars are shown in Table 1. The timestamp is created at the moment of ~~arrival~~ reception of the information. All parameters that originate from interrogation, have an observation frequency depending on the radar, ~~however~~ ADS-B information can have an observation frequency of twice per second.

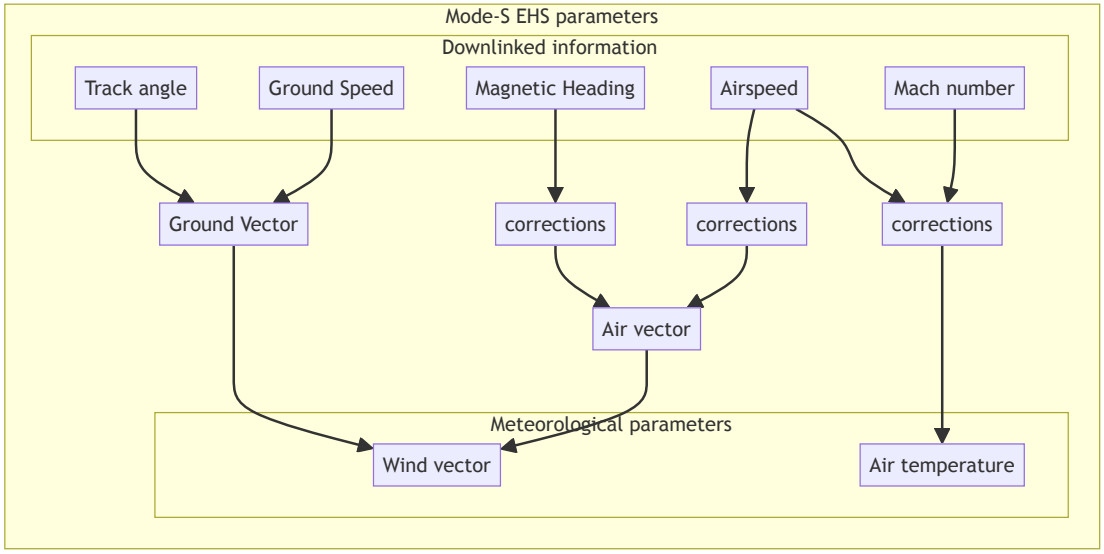

Figure 2. Downlinked data flow of Mode-S EHS ~~observations~~ parameters to acquire meteorological information.

Table 1. The reported ~~accuracy~~ precision and observation frequency of downlinked parameters, all parameters are rounded.

~~Barometric Altitude Rate bar 32 5s - 20s ft/min 6.0 Inertial Vertical Velocity ivv 32 5s - 20s ft/min 6.0 East-West Velocity gspd-u G'_u 1 0.5s - 2s knots 0~~

Table 1 displays ~~some information of~~ information on the downlinked parameters. The information flow of the downlinked parameters is depicted in Figure 2. Also shown in this figure are the corrections applied to the magnetic heading, true airspeed and Mach-number, discussed later.

Table 2. Current input quality checks used in operation.

	Input data quality checks	occurrence
1	absolute value of roll angle larger than 2.5 degrees ~~,~~	16%
2	absolute difference between track angle and magnetic heading larger than 25 degrees	1%
4	true air speed larger than 570 kts or smaller than 100 kts	1%
5	groundspeed larger than 850 kts or smaller than 50 kts, or when below flight level 50 smaller than 100kts	2%
6	Mach number ~~smaller than 0.001~~ equal to 0	2%
7	constant flight level and decreasing ground speed and indicated airspeed when ~~fl~~ flight level is lower than 50~~8~~	~~flightlevel lower than -100~~ 2%

4.2 Raw ~~data input control~~Data Input Control

The EMADDC quality procedure has been ~~developed and refined in the last~~ systematically developed and enhanced over the past decade. The first step in defining the quality is to check the input for obvious errors or measurements in conditions where calculation is not possible, as listed in Table 2. Measurements ~~fulfilling~~ failing one of these checks are discarded from further processing.

4.3 Output ~~control~~ Control and ~~whitelisting~~Whitelisting

Output control is necessary to obtain good quality observations. The parameters for output quality control are related to the ~~corrections~~ correction methods applied to the temperature and wind measurement.

Additionally, whitelisting is ~~performed to ensure that observations are within three times standard deviation of the measurement with NWP model equivalents. EMADDC currently uses the operational ECMWF IFS model for this comparison.~~

5 ~~Derived temperature~~

~~Although the temperature is measured by the sensors onboard the aircraft, the information is not transmitted in the Mode-S EHS request BDS5.0~~ conducted for wind speed and ~~BDS6.0. However, the Mach number M and the airspeed A are available and from these paramters the temperature can be deduced using the relation between the speed of sound and temperature and the ideal gas law,~~

$$M = \frac{A}{C},$$

~~where $C = \sqrt{\gamma R_d T}$, where $\gamma = c_p/c_v$ is the ratio of specific heats and R_d is the universal gas constant for dry air. Thus, given M and A, the temperature T can be calculated by~~

$$T = \frac{1}{\gamma R_d}\left(\frac{A}{M}\right)^2,$$

~~where A is in m/s.~~

4.1 ~~Temperature measurement improvements~~

~~The aircraft measurements are improved by algorithms onboard the aircraft. The applied corrections are not available and may be aircraft dependent, or aircraft type dependent, or both. It is known that the measurement of the static pressure p_s suffers from airflow instabilities and/or angle of attack (Rodi and Leon, 2012). The static pressure is corrected, which consequently results in a correction of the Mach number M and temperature$T$.~~

4.1 ~~Aircraft dependent temperature bias correction~~

~~A temperature correction is constructed using auxiliary temperature information, obtained from NWP. The temperature measurement depends on the Mach number, which in turn depends on pressure, and pressure, at low altitude, is less accurate. Therefore, an improved pressure value that would result in a measurement of~~ temperature ~~T, given the dynamic pressure q_t and true airspeed A. To accommodate this, for each aircraft these corrected values of pressure are stored and used to determine a relation between the corrected pressure, the original pressure and the true airspeed. In this a corrected temperature is obtained by recalculating the temperature with corrected pressure information, derived from the fit of the corrected pressure values by function p_{cor}. This function, which depends on pressure and true airspeed, is defined as~~

$$p_{cor} = a + bp_s + c\frac{p_s}{A^2}$$

~~where the coefficients a~~independently, based on the difference between observations and forecast statistics. Aircraft with a 14-day wind standard deviation exceeding 4 knots are designated as ineligible, while for temperature, ~~b and c are found by fitting and are aircraft dependent. The procedure used is described in more detail in de Haan et al. (2022)~~ the standard deviation threshold is set at 1.23 Kelvin. EMADDC currently uses the operational ECMWF model with a minimal forecast lead time of 9 hours for this comparison by collocating observations with NWP.

5 Derived ~~wind measurement~~Wind Measurement

The wind vector is the difference between ground vector and air vector, where all vectors are with respect to true North.

$$V\begin{pmatrix}\cos(d)\\ \sin(d)\end{pmatrix} = G\begin{pmatrix}\cos(t)\\ \sin(t)\end{pmatrix} - A\begin{pmatrix}\cos(h)\\ \sin(h)\end{pmatrix}, \tag{4}$$

where V denotes the wind speed with wind direction d. Note that this equation is valid under the assumption that the vertical wind speed is negligible, the sideslip is zero and the roll angle is small. The heading is reported with respect to the magnetic North Pole and needs to be converted into a heading with respect to true North. For this purpose, geomagnetic declination tables from (Maus and Macmillan, 2005; Chulliat, 2015) are applied, thus

$$h = h_m + \delta\Delta(y, \lambda, \phi), \tag{5}$$

where y is the the datum of the statc heading correction table on-board the aircraft, and, (λ, ϕ) is the location of the aircraft and ~~δ is the applied heading correction~~ Δ is the heading correction from the declination table. As it turns out, the heading correction is aircraft dependent, that is y is aircraft dependent, and even may change in time after an aircraft is being serviced, for example when the computer software is updated (Mirza et al., 2016).

5.1 Aircraft ~~dependent heading correction~~Dependent Heading Correction

Although the correction should be in the order of the (actual) declination, ~~previous research found~~ research showed that a simple correction is not enough ~~(de Haan, 2011). As it turns out, each~~ (de Haan, 2011; Pourret et al., 2021). Each aircraft may use ~~its~~ their own version of a declination lookup table, which implies that each aircraft corrects the true North to magnetic North in a different way. ~~Hence, the~~ The correction method uses the assumption that the correction is determined by a geomagnetic reference table for a certain datum (or epoch) and is static until updated through aircraft maintenance. The optimal datum is found by minimizing a cost function, depending on datum, by comparing corrected winds from observations with NWP model forecast winds. The cost function is constructed by the vector length difference between the unit heading vector from the aircraft and the unit heading vector formed by the ground vector and NWP-wind vector, that is

$$\delta^i(y) = \begin{pmatrix} \cos\left(h_N^i\right) - \cos\left(h_m^i + h_c\left(y, \lambda^i, \phi^i\right)\right) \\ \sin\left(h_N^i\right) - \sin\left(h_m^i + h_c\left(y, \lambda^i, \phi^i\right)\right) \end{pmatrix}, \tag{6}$$

with

$$h_N^i = \operatorname{atan}\left(\frac{G^i \sin\left(t^i\right) - V^i \sin\left(d^i\right)}{G^i \cos\left(t^i\right) - V^i \cos\left(d^i\right)}\right), \tag{7}$$

and i the index of an observation, h_m^i is the observed magnetic heading and $h_c(y(\lambda^i, \phi^i))$ the value of the declination table with datum y at location (λ^i, ϕ^i). The cost function is defined as the sum of all vector length differences over all observations, that is

$$\begin{aligned} C(y) &= \frac{1}{2}\sum_i ||\delta^i(y)||^2 && (8) \\ &= \frac{1}{2}\sum_i \left(\sin\left(h_N^i\right) - \sin\left(h_m^i + h_c^i(y)\right)\right)^2 + \left(\cos\left(h_N^i\right) - \cos\left(h_m^i + h_c^i(y)\right)\right)^2 && (9) \\ &= \sum_i 1 - \cos\left(-h_N^i + h_m^i + h_c^i(y)\right) && (10) \end{aligned}$$

Next, magnetic declination is linearized with datum, in order to find a minimum, that is

$$h_c^i = H_0^i + (y - y_{ref})\Delta H^i, \tag{11}$$

where H_0^i is the value of magnetic declination for given lat/lon on datum y_{ref}, ΔH^i value of the change in magnetic declination per year (this approximation is valid, as is discussed in Appendix A). ~~We approximate the cost function~~ The cost function is

approximated by a quadratic function in the datum offset, which yields

$$C(y) \approx 1 - \cos\left(H_0^i - h_N^i + h_m^i\right) + \delta_y \sum_i \frac{\left(\Delta H^i\right)^2 \delta_y^2 \cos\left(H_0^i - h_N^i + h_m^i\right)}{2} + \Delta H^i \sin\left(H_0^i - h_N^i + h_m^i\right) + \frac{1}{2}\delta_y \sin\left(H_0^i - h_N^i + h_m^i\right) - ^2 \sum \tag{12}$$

where

$$\delta_y = y - y_{ref} \tag{13}$$

The (offset) datum value for which the cost function attains a minimum is found by setting the derivative to δ_y of the cost function to zero. Let x_1^i and x_2^i for observation i be defined by

$$x_1^i = -\Delta H^i \sin\left(H_0^i - h_N^i + h_m^i\right) \tag{14}$$

$$x_2^i = \left(\Delta H^i\right)^2 \cos\left(H_0^i - h_N^i + h_m^i\right), \tag{15}$$

then the datum minimizing the cost function is given by

$$y = y_{ref} + \frac{\sum_i x_1^i}{\sum_i x_2^i} \tag{16}$$

Using the found datum for an aircraft ~~, EMADDC calculates the magnetic declination~~ EMADDC calculates using this datum the corresponding magnetic declination tables at the location of an observation to find the declination and converts the reported magnetic heading to true heading and calculate the wind according to the equation above.

5.2 ~~Dependence on NWP wind vector information~~

~~The~~

The above method uses NWP wind forecasts extracted from the operational ECMWF forecast. The forecast lead-time is at least 9 hours, such that observation from Mode-S EHS are not used as input for assimilation and correction simultaneously.

5.2 Heading Correction Results

Figure 3 shows the results of the heading correction for all 19006 aircraft operational in 2023. Each aircraft is represented by a vertical line in the top panel. The white colour indicates that no correction was found and aircraft with a lot of white pixels are not regular flying in the EMADDC domain. The top panel shows the offset with the maximum reported heading correction in 2023. In general, the change in heading correction over 2023 is small, except for aircraft that have high correction datum values. The most constant datum corrections values (offsets smaller than 2 years, red to brown colored) are found for values close to 2023, while higher offsets are only found with high maximum values, which gives reason to believe that for these aircraft the datum correction algorithm may not perform optimally.

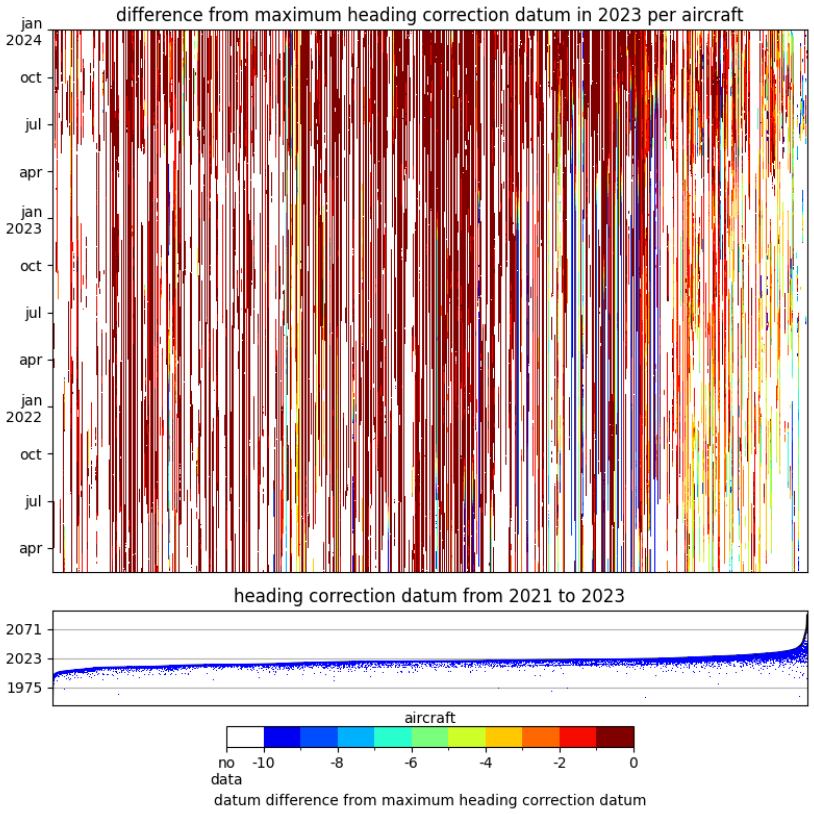

Figure 3. Top panel shows the difference of heading correction in 2023 with the reported maximum heading correction datum in 2023. The white color indicates that no (or bad) heading correction value was reported. The bottom panel shows the maximum heading correction found in 2023 (top black line) with the deviations from its maximum as small blue dots. The 19006 aircraft are sorted by maximum heading correction.

5.3 Dependence on NWP Wind Vector Information

The magnetic heading is calibrated using NWP wind vector information. Consequently, the obtained correction depends on the quality of the NWP information. The magnitude of this dependence is small, and of the order of one over the ~~ground speed.~~ magnitude of ground speed which is explained in the following.

Suppose we have a biased NWP wind direction, that is the true wind direction d is biased by β, then

$$\tilde{h}_N = \operatorname{atan}\left(\frac{G\sin(t) - V\sin(d+\beta)}{G\cos(t) - V\cos(d+\beta)}\right) \approx h_N + \frac{V\beta(-G\cos(d-t)+V)}{G^2 - 2GV\cos(d-t)+V^2}, \tag{17}$$

which implies that

$$|\tilde{h}_N - h_N| \lessapprox \left|\beta\frac{V(V+G)}{(G-V)^2}\right| \lessapprox \frac{|\beta|}{G} \ll |\beta|. \tag{18}$$

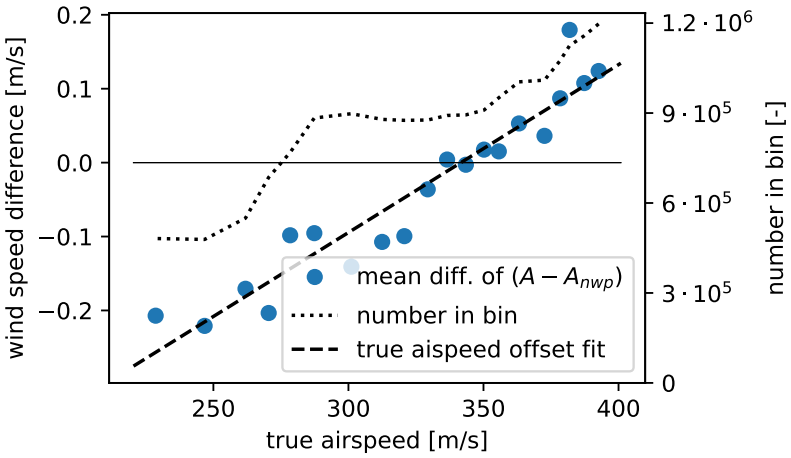

Figure 4. The mean difference of true airspeed as derived from observed ground vector and model wind versus the observed true airspeed. Data from three full days (2021/06/05, 2021/12/02 and 2023/08/01) and two 6 hours intervals (2022/08/01 06-12 UTC, and 2023/01/01 00-06 UTC) is shown.

The offset from the true heading using ~~wnd~~ wind direction biased information is substantially smaller ~~then~~ than the actual bias. Similarly the offset from the true heading based on wind speed biased (by α) is given by

$$|\tilde{h}_N - h_N| \lessapprox \left|\alpha \frac{G\sin(d-t))}{G^2 - 2GV\cos(d-t) + V^2}\right| \lessapprox \frac{|\alpha|}{G} \ll |\alpha|. \tag{19}$$

Since the heading correction is based on many of observations, over a large period (~~minimal~~ at least 15 days) it can be regarded as independent of the NWP information.

5.4 True ~~airspeed correction~~Airspeed Correction

The measurement of true airspeed depends on the temperature and Mach number, see ~~equation (??~~Equation (3). Since the observed Mach number is corrected (Rodi and Leon, 2012), the true airspeed ~~observation can~~ measurement might be improved likewise. ~~The EMADDC~~

The current algorithm uses an aircraft dependent constant correction value. However, in the next processing version a true airspeed dependent true airspeed correction will be implemented. This improvement is reasoned by comparing the observed true airspeed with a model true airspeed as a function of true airspeed. The model true airspeed is obtained by the vector difference between the observed ground vector and wind vector from the model. Figure 4 displays the average difference of the observed true airspeed versus the model-based true airspeed. The differences are averaged over true airspeed bins for all data points observed in the EMADDC domain in three days. Note that the difference in wind speed is of the order of a few tenth meter per second. Clearly there is a relation between mean airspeed difference and the true airspeed itself.

As a first order approach the EMADDC system currently applies a true airspeed bias correction depending on aircraft and phase of flight. Future research is foreseen to come to a physical method of true airspeed correction. Care must be taken when model based bias correction are applied because model biases themselves might bias the corrected observation. It all depends on the way the biases are related.

6 ~~Processing Infrastructure~~Derived Temperature

~~EMADDC suppliers currently provide data in 5-to-15-minute batches where the system picks up~~ Although the temperature is measured by the sensors onboard the aircraft, the information is not transmitted in the Mode-S EHS request BDS5.0 and BDS6.0. However, the Mach number M and the true airspeed A are available and from these parameters the temperature can be deduced using the relation between the speed of sound and temperature and the ideal gas law,

$$M = \frac{A}{C}, \tag{20}$$

where $C = \sqrt{\gamma R_d T}$ and R_d is the universal gas constant for dry air. Note that the dependence of the speed of sound on humidity is neglected. So, given M and A, the temperature T can be calculated by

$$T = \frac{1}{\gamma R_d}\left(\frac{A}{M}\right)^2, \tag{21}$$

where A is in [m/s].

6.1 On Board Aircraft Temperature Correction

The aircraft measurements are improved by algorithms onboard the aircraft. The applied corrections are not available and may be aircraft dependent, or aircraft type dependent, or both. It is known that the measurement of the static pressure p_s suffers from airflow instabilities and/or angle of attack (Rodi and Leon, 2012). The static pressure is corrected, which consequently results in a correction of the Mach number M and temperature T.

6.2 Temperature Measurement Improvements

The temperature is calculated from the Mach number and the true air speed on-board of the aircraft. Actually, there are two types available of the Mach number, one being the downlinked data and one determined using indicated airspeed information. The downlinked Mach number is of worse accuracy than the Mach number determined from the indicated airspeed, as will be discussed next. An estimate of the formal error of the temperature T calculated using Equation 21 is constructed following (Taylor, 1997),

$$\sigma_T^2 \approx \left(\frac{\partial T}{\partial A}\right)^2 \sigma_A^2 + \left(\frac{\partial T}{\partial M}\right)^2 \sigma_M^2 = \frac{4T^2}{A^2}\sigma_A^2 + \frac{4T^2}{M^2}\sigma_M^2 \tag{22}$$

Rounding leads to an additional error of $r/\sqrt{12}$, where r is the rounding (see Appendix B). One of the downlinked parameters is indicated airspeed which is defined as the airspeed measured as if the aircraft was flying at mean sea level ($p_0 = 1013.25$hPa, $T_0 = 288.15$, and $\rho_0 = 1.225$kg/m^3, the standard pressure, temperature and density at mean sea level)

$$A_I = \sqrt{\frac{2}{\gamma-1}\frac{p_0}{\rho_0}\left(\left(\frac{q_t}{p_0}+1\right)^{\frac{\gamma-1}{\gamma}}-1\right)} \Rightarrow q_t = p_0\left(\left(\frac{\gamma-1}{2}\frac{\rho_0}{p_0}A_I^2+1\right)^{\frac{\gamma}{\gamma-1}}-1\right) \tag{23}$$

The dynamic pressure q_t can be calculated from A_I, which in turn can be used to recalculate M, according to Equation (1), an (first order) estimate of the error in Mach number can be obtained,

$$\sigma_M^2 \approx \left(\frac{\partial M}{\partial q_t}\frac{\partial q_t}{\partial A_I}\right)^2 \sigma_{A_I}^2 \tag{24}$$

$$\approx \frac{A_I^2}{M^2}\frac{\rho_0^2}{p^2}\left(1+\frac{q_t}{p}\right)^{-\frac{2}{\gamma}}\left(\frac{A_I^2\rho_0(\gamma-1)}{2p_0}+1\right)^{\frac{2}{\gamma-1}}\sigma_{A_I}^2 \tag{25}$$

Figure 5 shows the formal temperature errors as calculated with the downlinked Mach number ($\sigma_T^2(M)$, red line) and the temperature error based on the indicated airspeed ($\sigma_T^2(A_I)$, dashed blue line), and the formal error term related to the A. The effect on introducing the Mach indicated airspeed is a reduction in formal error of a factor of 4. The largest part in the formal error is (with the A_I) is now related to the true airspeed error. This implies that to further improve the temperature observation reduction of true airspeed error needs to be accomplished. The temperature correction is performed in two steps: first averaging

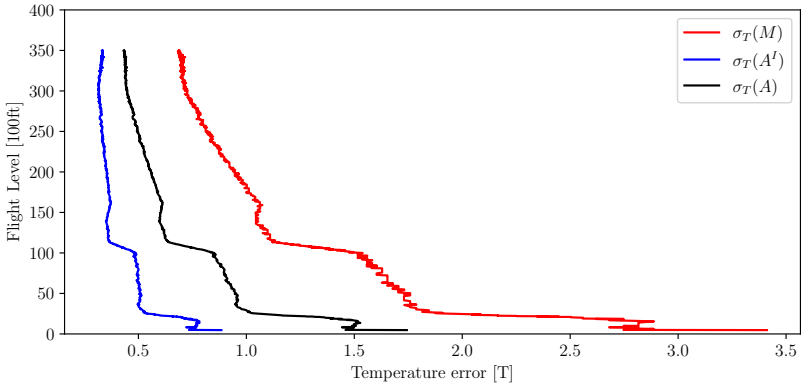

Figure 5. Different terms of the formal error for temperature. Black line represents the formal error due to uncertainty in A; the term related to the temperature derived using the (coarse) Mach number, and, blue line depicts the formal error when the Mach number is recalculated from A^I. Aircraft data from ICAO24 A2BD72 (Airbus A320-214), valid from 2023-08-01 05:17:07 to 2023-08-01 05:26:40

and followed by a correction. An average over 20 seconds is determined to reduce the noise in the temperature observation,

that is

$$\overline{T} = \frac{1}{N}\sum_{i}^{N} T_i^I, \tag{26}$$

and average observations are marked as bad when the standard deviation of the observations T_i^I exceeds 5K.

The temperature correction applied is based upon correcting the static pressure measurements and recalculating subsequently the Mach number, the total temperature and finally the temperature. The correction used is described in detail in de Haan et al. (2022) . The corrected static pressure correction p_c depends on the static pressure itself, and the static pressure divided by the square of true airspeed, that is

$$p_c = a + p_s\left(b + \frac{c}{A^2}\right), \tag{27}$$

where the a, b and c are determined by fitting NWP temperatures. These coefficients are aircraft dependent. The corrected temperature is determined as follows: first the corresponding total temperature is calculated,

$$\overline{T}_t = \left(1 + \lambda\frac{(\gamma-1)}{2}M^2\right)\overline{T}, \tag{28}$$

and then the corrected temperature calculated using the corrected pressure p_c becomes

$$\overline{T}_c = \left(1 + \lambda\frac{(\gamma-1)}{2}M_c^2\right)^{-1}\overline{T}_t, \tag{29}$$

where

$$M_c^2 = \frac{2}{\gamma-1}\left(1 + \frac{q_t}{p_c}\right)^{\frac{\gamma}{\gamma-1}} - 1 \tag{30}$$

Figure 6 displays the effect of the three steps (green 'raw' temperature, improving M by the indicated airspeed (red), followed by the averaging (blue) and pressure correction (black)). Applying a simple smoothing of adjacent points, the standard deviation is reduced to values between 1 [K] in mid-troposphere and growing to 1.5 at higher altitudes and near the surface (Figure 6 compare red and black dashed lines); The bias (and standard deviation to less extend) is then further reduced by applying the raw pressure correction method (Figure 6 black lines).

Figure 7 displays the neccessary steps needed in the processing to turn Mode-S EHS observations into meteorological information.

7 Data Processing Methodology

EMADDC suppliers generally deliver data in batches every 5 to 15 minutes, allowing the system to retrieve new files for ~~ingesting~~ ingestion into the EMADDC database. ~~For receiver data , the data is handled~~ The receiver data is processed by the

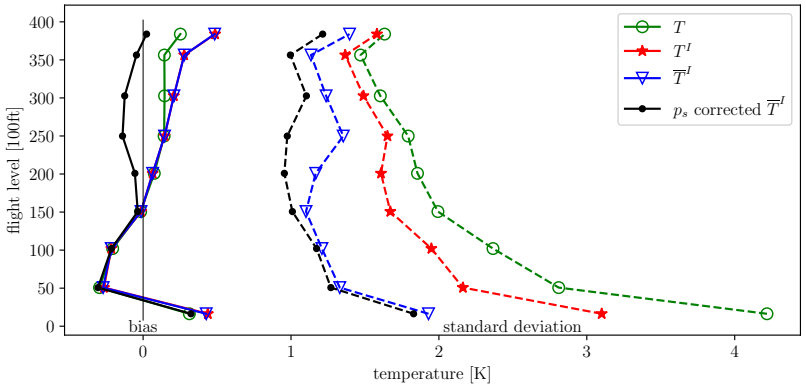

Figure 6. Results of temperature correction based on data from 2023-08-01 06-12UTC. Red line depicts the mean difference between model and observation (solid line) and standard deviation of the difference (dashed line). The blue line represents the time averaging statics, while the black line is the result after the raw pressure correction.

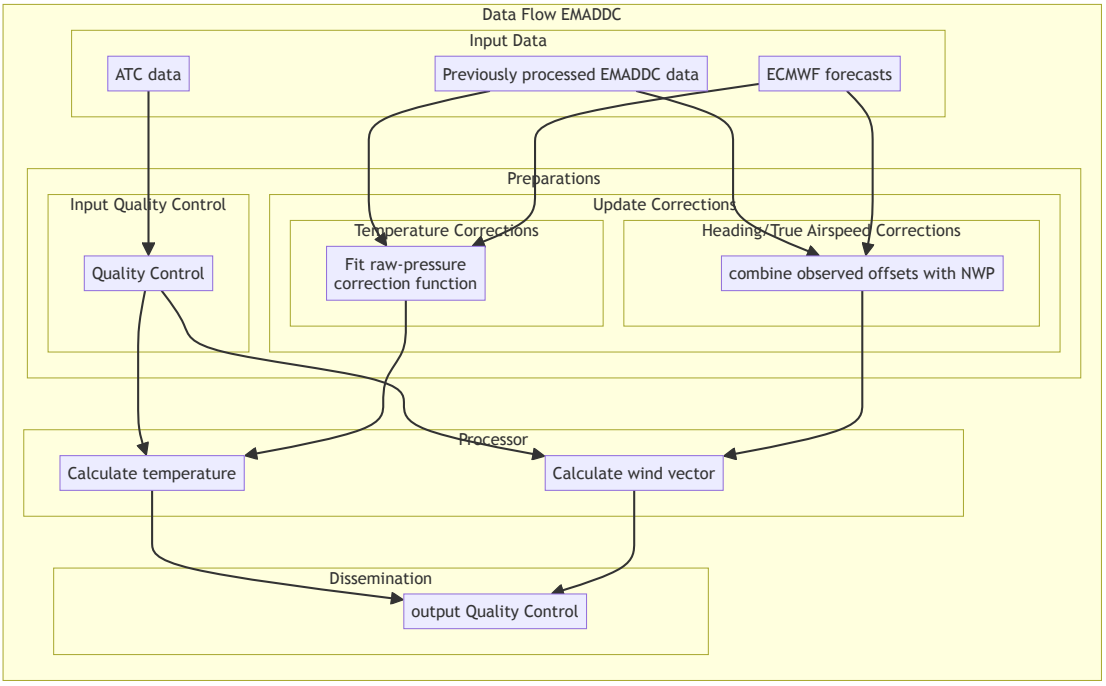

Figure 7. Functional data flow in EMADDC, needed to derive wind vector and temperature observations.

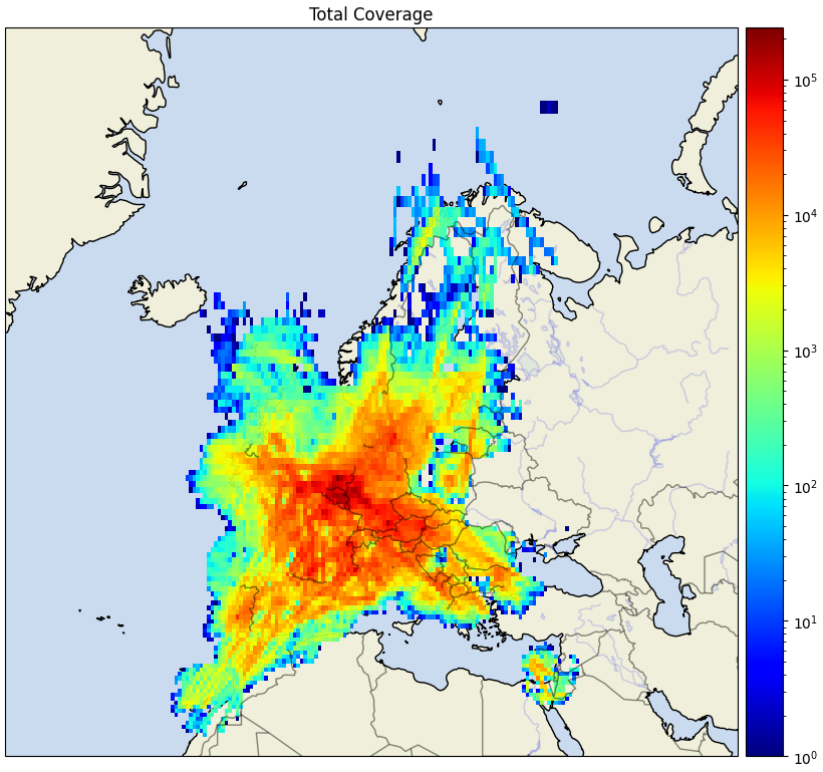

Figure 8. Data coverage of Mode-S EHS ~~observatons~~ on April 21st 2024. The color indicates the number of observations per 0.5 degrees squared box.

decoder~~and combined to create observations from~~ , which combines the BDS5.0 and BDS6.0 registers ~~received and insert these~~ to generate observations that are subsequently entered into the EMADDC database. In contrast, for ATC radar/tracker data, the observations are decoded (from ASTERIX to an EMADDC internal format) and inserted into the database. For this type of data, no intermediate combining step is necessary, as the registers have already been consolidated by the respective tracker or radar system.

Once ~~data is ingested into an hourly~~ the data has been ingested into the hourly database table, the processing scheduling system ~~schedules three jobs. One processing job that contains observations of a 15 minute time windowwith a delay of approximately~~ triggers three specific processing jobs. The first job handles observations within a 15-minute time window, operating with an approximate delay of 30 minutes. This job functions as the primary processing task, indicating that the designated time window has been successfully processed.

In 2022, two ~~new processing jobs that process~~ additional processing jobs were introduced to process observations in 5-minute batches at 13 and ~~23-minutes past the first observation in a time windowhave been added to the system. These "fast" files provide about~~ 23 minutes past the initial observation in the designated time window. These "fast" files account for approximately 70% and 90% of ~~all data that is~~ the total data available in the ~~regular and existing~~ standard 15-minute interval files~~.~~ , respectively. The implementation of these new fast files has notably enhanced the timeliness of EMADDC by reducing the delivery delay to approximately 10 minutes. These fast files should be utilized when 15-minute interval data is not yet available/processed.

A processing job ~~starts by gathering all data available in the time window of interest~~begins by collecting all available data within the specified time window. The input data ~~is quality controlled, as discussed before. The last 5~~ undergoes quality control, as previously outlined. To ensure continuity in flight profiles and phase determination, the data from the last five minutes of the ~~previous~~ preceding time window is ~~prepended~~ included for continuation of flight profiles and phase determination. The flight profile and flight phase are used when applying the corrections. Wind and temperature are derived using equations for wind speed and wind direction (see above), the detected magnetic table datum is used in the World Magnetic Model (Chulliat, 2015) to determine the magnetic declination at the location of the observation and obtain the true heading. ~~The other~~ Subsequent corrections and post-processing ~~is subsequently applied~~are applied, after which outliers are ~~detected using a 30 seconds rolling window and median and 3 standard deviation outlier detection~~identified using linear regression over individual aircraft's 30-second time windows.

EMADDC currently receives data from multiple overlapping sources. For ~~example, for~~ instance, in the EUROCONTROL MUAC area, EMADDC ~~receive~~ obtains radar data from MUAC ~~but also receiver data from 8 receivers from AirSupport. KNMI has a receiver at de Bilt and one at Cabauw at 180m receiving data up~~ as well as data from approximately eight receivers operated by ADSB Support. KNMI operates receivers located in De Bilt and Cabauw at 180 meters, which capture data extending to Paris. Since ~~technically these receivers receive the same data as the radars at ATC, EMADDC has duplicity in its database . Therefore~~ these receivers collect similar data to that of the radars used in ATC, the EMADDC database contains duplicate entries. To address this issue, a duplicate detection algorithm ~~is applied where~~ has been implemented, whereby data from the same aircraft ~~within 1~~ recorded within one second of another observation is ~~marked as~~ designated as a duplicate of the primary observation. ~~Note, that observation retrieved~~ Observations identified as duplicates are not included in the EMADDC output. It is important to note that observations obtained directly from Air Traffic Control~~directly (~~—such as radar or tracker data~~) is never marked as a duplicate observation as ATC system apply~~ —are not marked as duplicates, as the ATC system applies its own filtering and quality control ~~on their end and remove duplicates. Hence, it can occur that an observation is present~~ measures to eliminate duplicates. Consequently, it is possible for an observation to appear in a fast file, but ~~later is no longer available in the subsequent (~~be absent in subsequent 23-minute ~~) fast file~~ fast files or full time-window ~~file as it was marked~~ files if it was identified as a duplicate and replaced by another observation. The current approach to identifying duplicates has demonstrated effectiveness; however, it is not without imperfections. The intent is to enhance this process in future developments of EMADDC R3.0. In addition to this step of identifying duplicate observations, the decoding and combining process effectively addresses the potential for duplicate registers that may be received from multiple overlapping

receivers within a receiver file. Furthermore, ATC data does not contain duplicate observations, as radars exclusively process received interrogations that pertain to their own interrogations, discarding those produced by other radars. ~~The last processing step is to check whether~~

The final processing step involves verifying whether the observations are from aircraft that have been ~~whitelisted. Whitelisting is performed for wind speed and temperature separately and is based on observations minus forecast statistics. Aircraft for which the 14-day standard deviation exceeds 4 kts are blacklisted while for temperature the standard deviation limit is set at 1.23 K. Finally, all valid and quality checked data is outputted in ASCII, NETCDF and BUFR files and is made available using KNMIdata platform~~approved for use through whitelisting as explained in Section 4.3.

Ultimately, all validated, non-duplicate, and quality-checked data are compiled into CSV and BUFR file formats. These files are be made accessible via KNMI's FTP servers and the KNMI Data Platform (KDP)[1]. Access to these files or datasets is currently restricted to authorised users and the intent is for EMADDC to provide (some) observations as "open-data" in the future.

8 Results

Produced observations are continuously validated against the model and radiosondes. The ~~tables below~~ next section show the numerical weather prediction statistics over three months (January - March 2024)~~and~~ ; Section 8.2 discusses Mode-S EHS versus radiosondes (January - March 2023) ~~.~~(and NWP). And in Section 8.3 Mode-S EHS, AMDAR and NWP are compared over an eight month period.

8.1 Model ~~comparison~~Comparison

In three months, a total ~~4.5 of~~ of 4.5 billion observation were ~~collected~~ derived by the EMADDC system. From these observations 2.8 billion unique and whitelisted wind observations are made available to the users, and in total nearly ~~1,8~~ 1.8 billion temperature observations are disseminated in three months. The quality of wind observations compared to ECMWF-IFS is around 2.5 [m/s] in standard deviation, with a small bias of 0.3 [m/s], see table 3. Table 3 also shows the statistics of wind and temperature observations for different height levels: the error in wind speed with respect to the model increases with height from 2.2 [m/s] near surface to 2.8 [m/s] at a height of 11 km. The wind direction statistics show a different signal; near the surface the wind direction error is nearly 15 degrees, with a minimum at around flight level 350 and increasing again to an error of 10 degrees at around 11 km. Note that only observations with wind speed larger than 4 m/s are used for wind direction. Wind is in general more variable near the surface. These values are all within the acceptable range for use in for example data assimilation.

The temperature statistics are shown in Table 4. The temperature error in total is slightly smaller than 1 [K], with a minimum ~~of~~ error of 0.8 [K] around flight level 250. The maximum error is found at cruising level (11 km). Note that the bias with the model is around to zero.

[1]Please visit https://dataplatform.knmi.nl/dataset/access/emaddc-hist-repro-data-1-0

Table 3. Statistics of EMADDC wind observations against the operational ECMWF model

		January 1, 2024 to April,1 2024				
			wind speed, EHS - NWP			wind dire
		raw volume	number	bias [m/s]	std.dev [m/s]	number
~~all data~~	all data	4 546 047 080	4 384 070 442	0.34	4.76	4 281 120 981
~~whitelisted and unique~~	whitelisted and unique	2 868 355 459	0.30	2.52	2 800 011 753	0.17
flight level	pressure (hPa)	raw volume	number	bias [m/s]	std.dev [m/s]	number
0-100	1013 - 696	235 608 797	151 947 715	0.20	2.20	135 707 126
100-200	696 - 465	361 851 780	252 516 206	0.22	2.28	243 224 271
200-300	465 - 300	594 829 968	386 369 304	0.27	2.53	378 271 790
300-400	300 - 187	3 133 630 884	2 016 820 254	0.32	2.60	1 983 182 045
>400	<187	220 023 701	131 427 728	0.36	2.81	128 500 903

Table 4. Statistics of EMADDC temperature observations against the operational ECMWF model

	January 2024 - March 2024				
			temperature, EHS - NWP		
	~~raw input temperature~~	raw input	number	bias	std.dev
~~all data~~ all data	4 546 047 080	3 138 758 482	0.02	1.05	
~~whitelisted and unique~~ whitelisted and unique	-	1 763 880 586	-0.00	0.95	
flight level	pressure (hPa)	raw volume	~~bias~~ number	bias [K]	std.dev [K]
0-100	1013 - 696	235 608 797	51 837 791	0.13	1.08
100-200	696 - 465	361 851 780	140 307 524	0.05	0.83
200-300	465 - 300	594 829 968	241 388 676	0.06	0.77
300-400	300 - 187	3 133 630 884	1 309 098 407	-0.01	1.04
>400	<187	220 023 701	83 204 202	0.05	1.24

8.2 Comparison with ~~Radiosondes observations~~Radiosonde Observations

Radiosondes are regarded as ~~the~~ anchor observation for meteorology and are generally launched at the main synoptic hours 00 UTC and 12 UTC, with ~~some~~ few sites launching also at 06 UTC and 18 UTC. Due to budget ~~optimization, the number of launches per daywas decreased to one or two~~restrictions some radiosondes are only launched once a day. Aircraft observations are regarded as ~~replacement to collect~~ supplemental upper air observations of wind and temperature. ~~The table below~~ Table 5 shows collated observations statistics of wind (wind speed, and the wind components) and temperature. Aircraft and observations will never be exactly collocated in both space and time~~, moreover aircraft are warned when a nearby meteorological station launches a balloon, and avoids the balloon.~~ . Nevertheless, collocations can be made by having the maximum distance

Table 5. ~~Comparison~~ Statistics of wind observations comparison against Radiosondes

Jan 2023 - March 2023

East-West wind component [m/s]

			EHS - RS		EHS - NWP		RS - NWP	
flight level	pressure(hPa)	number	bias [m/s]	std.dev [m/s]	bias [m/s]	std.dev [m/s]	bias [m/s]	std.dev
< ~~50~~ 0	~~160 746~~ > 1023	~~0.11~~ 166	~~2.75~~ 0.58	~~0.24~~ 1.16	~~2.79~~ 0.40	~~0.19~~ 1.41	~~2.72~~ 0.09	
~~50 < 150~~ 0 - 100	~~434 029~~ 1013 - 696	~~0.09~~ 541 153	~~2.13~~ 0.07	~~0.17~~ 2.42	~~2.40~~ 0.20	~~0.23~~ 2.59	~~2.24~~ 0.19	
~~150 < 250~~ 100 - 200	~~565 086~~ 696 - 465	~~0.12~~ 790 741	~~2.16~~ 0.11	~~0.10~~ 2.08	~~2.42~~ 0.11	~~0.14~~ 2.32	~~2.28~~ 0.17	
~~250 < 350~~ 200 - 300	~~858 477~~ 465 - 300	~~0.08~~ 976 001	~~2.21~~ 0.10	~~0.03~~ 2.25	~~2.62~~ 0.09	~~0.09~~ 2.66	~~2.47~~ 0.14	
~~350 < 450~~ 300 - 400	~~590 015~~ 300 - 187	~~0.04~~ 1 548 851	~~2.45~~ 0.05	~~0.04~~ 2.36	~~2.65~~ 0.06	~~0.07~~ 2.69	~~2.51~~ 0.11	
~~450~~ > 400	<187	~~236~~ 54 193	~~1.55~~ 0.09	~~2.42~~ 2.78	~~0.81~~ 0.10	~~1.98~~ 2.87	~~3.08~~ 0.04	~~3.56~~

North-South wind component [m/s]

< 50	>843	160 746	0.02	2.38	-0.06	2.47	-0.25
50 < 150	843 - 572	434 029	0.02	2.12	0.00	2.31	-0.09
150 < 250	572 - 376	565 086	0.02	2.27	-0.17	2.44	-0.22
250 < 350	376 - 238	858 477	0.01	2.33	-0.25	2.71	-0.23
350 < 450	238 - 147	590 015	-0.13	2.51	-0.32	2.78	-0.18
450 <	<147	236	0.03	1.92	-0.19	2.02	-0.17

~~< 50~~	~~160 746~~	~~0.03~~ Vector RMSE			
	~~2.82~~	~~0.39~~ EHS - RS	~~2.74~~ EHS - NWP		~~0.39 2.65~~RS - NWP
~~50 < 150~~	~~434 029~~ number	~~0.09~~ VRMSE [m/s]	~~2.13~~ VRMSE m/s	~~0.43 2.37 0.53 2.20~~VRMSE [m/s]	
~~150 <~~ 250 0	~~565 086~~ 166	~~0.21~~ 2.18	~~2.27~~ 2.06	~~0.44 2.44 0.58 2.35~~2.05	
~~250 < 350~~ 0 - 100	~~858 477~~ 541 153	~~0.07~~ 3.31	~~2.37~~ 3.53	~~0.45 2.74 0.49 2.59~~3.35	
~~350 < 450~~ 100 - 200	~~590 015~~ 790 741	~~0.19~~ 2.98	~~2.54~~ 3.32	~~0.62~~ 3.10	
200 - 300	~~2.80~~ 976 001	~~0.42~~ 3.30	~~2.67~~3.81	3.66	
~~450 <~~ 300 - 400	~~236~~ 1 548 851	~~1.53~~ 3.40	~~2.55~~ 3.89	~~0.87~~ 3.70	
> 400	~~1.91~~ 54 193	~~3.10~~ 3.84	~~3.47~~4.19	3.88	

between aircraft and radiosondes of at most ~~of~~ 50 km and maximum height difference of 100 m and time difference of 1800 seconds. ~~The table below shows the statistics of wind (wind speed, and the wind components) and temperature.~~

For all wind parameters, the comparison between radiosonde and Mode-S EHS ~~show to have~~ has a standard deviation lower than that of the comparison ~~is~~ model and Mode-S EHS or radiosonde. Furthermore, the difference between model and radiosonde or model and Mode-S EHS are similar and of the order of 0.3 to 0.5 m/s, while the mean difference between aircraft and balloon is small. Reason for this is that the model resolving resolution is in the order of 5 times the grid size, that is around 50km, while the observations measurements are close to in-situ. The temperature statistics show that all three systems have the

Table 6. Comparison against ~~Radiosondes~~Radiosonde

			Jan 2023 - March 2023				
			Temperature [K]				
~~< 50~~	~~11 635~~	~~0.00~~	~~1.45~~ EHS - RS	~~-0.01~~ EHS - NWP	~~1.54~~ RS - NWP		
flight level	~~-0.05~~ pressure(hPa)	~~1.19~~number	bias [K]	std.dev [K]	bias [K]	std.dev [K]	bi
~~50 <~ 150~~ 0 - 100	~~76 334~~ 1013 - 696	~~0.06~~ 165 790	~~0.96~~ 0.03	~~-0.01~~ 1.17	~~0.97~~ 0.05	~~-0.11~~ 1.13	~~0.77~~ -0.(
~~150 < 250~~ 100 - 200	~~71 541~~ 696 - 465	496 154	0.07	~~0.80~~ 0.84	~~0.01~~ -0.00	~~0.78~~ 0.84	~~-0.05~~ -0.(
~~250 < 350~~ 200 - 300	~~111 700~~ 465 - 300	~~-0.00~~ 704 675	~~0.89~~ -0.01	~~0.90~~ 0.76	~~0.01~~ 0.04	~~0.71~~0.78	0.(
~~350 < 450~~ 300 - 400	~~129 903~~ 300 - 187	~~0.05~~ 1 158 841	~~1.14~~ 0.01	~~-0.04~~ 1.04	~~1.10~~ -0.01	~~-0.10~~ 6.47	~~1.02~~ -0.(
~~450 >~ 400	<187	~~23~~ 36 737	~~-0.32~~ 0.08	~~1.13~~ 1.31	~~-0.77~~ 0.02	~~1.03~~ 1.27	~~-0.38~~ -0.(

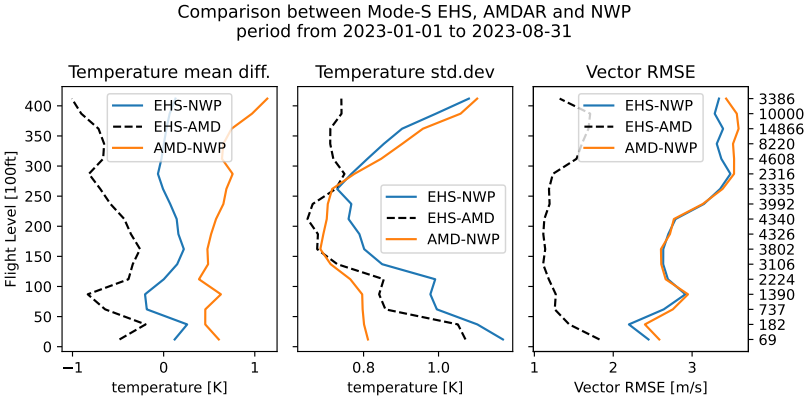

Figure 9. Statistics of an eight month period of collocated AMDAR and Mode-S EHS observations. Left panel shows the mean differences in flight bins of 25 ft; middle pane shows the standard deviation of the differences in temperature; the right panel shows the Vector RMS with respect to height.

same main temperature (all biases are small and near zero). Not surprisingly, the temperature observations of Mode-S EHS are clearly of less quality than radio soundings, although above ~~858~~ 850 hPa the quality is reasonable. ~~This~~

8.3 Comparison with AMDAR Observations

Finally, a comparison is made between Mode-S EHS observation and AMDAR observations. Figure 9 shows the statistics of Mode-S EHS, AMDAR and NWP for temperature and Vector RMSE. A database is used to connect AMDAR aircraft to an ICAO aircraft identification. This database is partially based on E-AMDAR information and is completed with results from collocation with Mode-S EHS observations. Due to rounding of position and time exact collocations of AMDAR and Mode-S can be tedious. Moreover, the reporting observation frequencies are different resulting in about half of the AMDAR observations being collocated. Here an AMDAR observation is close to a Mode-S EHS observation when the time difference

is less than 2 minutes, the distance is less than 1 km, and most importantly the height difference is at most 25 ft. The emphasise is on height, because in general temperature and wind tend to change more with height, than with horizontal displacements.

The temperature of AMDAR has a positive bias, when compared to NWP which is known in literature (Zhu et al., 2015) . The bias of Mode-S EHS is around zero. The AMDAR temperature standard deviation is clearly better than Mode-S EHS. The increase of standard deviation near the ground is due to atmospheric turbulence being more present near the surface (Schwartz and Benjamin, 1995).

For wind the Vector RMSE shows that both AMDAR and Mode-S EHS perform equally well; there are small differences, but not significant. However, a gross error check on the zonal wind is needed to because of systematic errors in B787 aircraft (WMO, 2022).

9 Conclusions and Outlook

This paper presents the ~~EMADDC system~~ current EMADDC system (R2.2) to produce wind and temperature observations derived from Mode-S EHS aircraft ~~observations.~~ messages.

Mode-S EHS is a surveillance method which not only tracks an aircraft in the range of the radar ~~. It also contacts~~ but it also interrogates the aircraft and ~~request special~~ requests specific information which is used by ~~surveillance~~air traffic services. This downlinked data contains sufficient information to derive wind and temperature at very high spatial and temporal resolution. ~~To~~ This data is being processed by EMADDC to produce high quality meteorological information. First of all, to be able to generate observations of good quality, several ~~corrections and~~ quality checks are applied. ~~One of the important corrections is the~~ The quality of directly derived wind and temperature is hampered by an unknown offset (in case of heading correction) or low resolution of the Mach number (when deriving temperature).

To obtain high quality wind measurements, a correction from magnetic heading to true heading is neccessary; this heading correction is unique for each aircraft ~~individually.~~

~~As a reference, the~~ and may change in time due to maintenance of the aircraft. The observations are compared to wind forecast of ECMWF ~~IFS modelis used~~model, radiosonde wind observations over a three month period and AMDAR observations over a period of eight months. The derived wind observations ~~are of good quality compared~~ compare well to the model ~~forecast. Note that, although the data is corrected using ECMWF forecast, the data is independent because a forecast lead time of minimal 9 hours is used, so that observation from Mode-S EHS are not used as input for assimilation and correction simultaneously.~~ and the radiosonde observations with similar statistics as when comparing AMDAR to model equivalents.

~~The temperature correction is~~ The temperature is derived from the quadratic quotient of the true airspeed and the Mach number, both values are truncated. The estimate of the Mach number can be improved by exploiting the downlinked indicated airspeed. Next, a mean temperature is determined using a 20 second time window, and finally, the temperature is corrected based on the methodology developed in de Haan et al. (2022). ~~As a reference temperature again the ECMWF IFS model is used~~Error analysis revealed that the quality of the true airspeed measurement limits the temperature quality. Comparison with radiosonde observations showed good quality with respect to temperature when the ~~obervation~~ observation is above 850hPa.

AMDAR comparison showed that wind observations from Mode-S EHS are of equal quality, while temperature observations have 25% larger error. The produced meteorological information, when thinned to avoid overfitting, is widely used in limited area models and some global numerical weather prediction models.

A final remark needs to be made on the use of NWP forecast for correction. It is assumed that the NWP model and forecast are (almost) bias free. If this would not be the case then the bias might be reflected with reduced magnitude as a bias in the 'corrected' observations (Eyre, 2016). This paper showed that this is not the case for the heading correction because aircraft heading is not related to forecast values.

9.1 Outlook

The EMADDC team tries to improve the quality of derived wind and temperature continuously. The team has the following items to investigate or implement

- the current heading correction algorithm does not detect changes in the heading table datum effectively, especially when high datum correction values are detected; revisit of the heading correction algorithm is foreseen in the near future,
- applying a general true airspeed correction for both wind and temperature,
- similarly to temperature measurements, a formal error can be derived for wind observations,
- information on the formal errors are of great interest for users in data assimilation and EMADDC is looking into ways to disseminate this information,
- the vast volume of data per time period and region needs proper treatment for use in for example data assimilation, moreover incorporating formal errors correctly could be accounted for. Research within EMADDC is ongoing on how to apply this most efficient. Possible methods that will be applied are thinning, and/or super-obbing,
- the ADS-B information contains also geodetic height information, which might be valuable for data assimilation. Also information about the aircraft category and positional accuracy is available. The EMADDC team intents to add this information to the observation set created,
- the current system is file based, in near future a (near) real time production is foreseen using the real time networks of ATC in Europe (NewPENS) and real-time transmission of receiver data to EMADDC,
- as part of an initiative of Met Office end KNMI, EMADDC Met Office Global is processing data from Flightradar24 to enhance "global coverage" (limited to aircraft trajectories where Mode-S EHS is actively interrogated). The observations generated through this process are made available as CSV, NETCDF, and BUFR files exclusively to National Meteorological Hydrological Institutes. In time, these observations will be processed within the regular EMADDC system to accomplish synergy for corrections and to prevent data duplication and redundancy.

In the future ADS-B is foreseen to broadcast meteorological information (Rodriguez, 2023) creating enormous data volumes which are expected to require quality control of some kind for use in meteorological applications. The EMADDC system could fulfil the future quality assurance function.

Data availability. The processed historical data is available through the KNMI Data Platform https://dataplatform.knmi.nl.

Appendix A: Geomagnetic ~~data~~Data

This Appendix shows that the linear approximation in datum is valid for the domain of the current EMADDC processing.

The datum 2015/1/1 was set as the reference datum for the declination table in the current processing setup (~~version 2.2~~ R2.2 August 2023). The Geomagnetic model is used in determining the declination for a given position and time (Maus and Macmillan, 2005). Figure A1 shows the value of the declination on 2015/1/1 (left panel), the middle panel shows the yearly change ~~in declination,~~ and the right panel shows the difference between declination valid for 2020/1/1 and the linear approximation. The values of magnetic declination in central Europe are small. The change in declination is strongest for high latitude regions and close to zero for low latitude regions (middle panel). The error made by the linear approximation is small, as can be seen from the right panel.

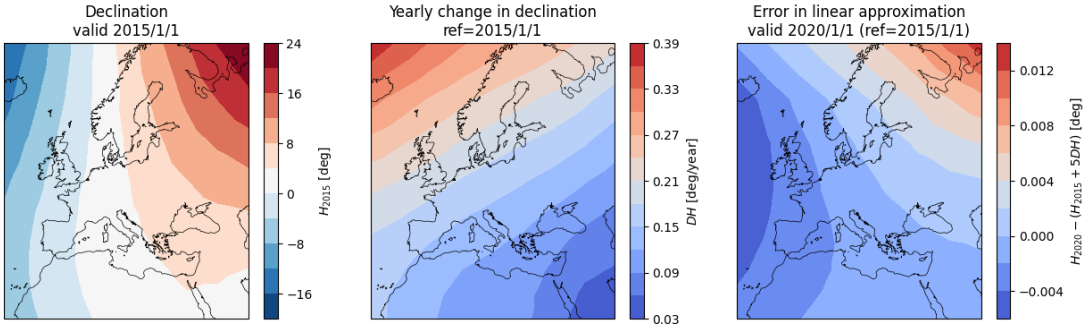

Figure A1. The effect of linearization of the declination around the datum 2015. Left panel the declination at 1st Jan. 2015; middle panel the yearly change on 1st Jan. 2015; right panel the difference between linearization and model declination on 1st Jan. 2020. Note that the contours differ for the three panels.

Appendix B: ~~Data sources~~Rounding Error

The error due to rounding is estimated as follows. Assume that the error of an measurement X is normal distributed with zero mean around the true value X_t, and standard deviation σ. The mean and second moment of the error in X are given by

$$\mathcal{E}(X - X_t) = \int_{-\infty}^{\infty} x \rho_X(x) dx = 0 \tag{B1}$$

$$\mathcal{E}((X - X_t)^2) = \int_{-\infty}^{\infty} x^2 \rho_X(x) dx = \sigma^2. \tag{B2}$$

Let $[X]_r$ be the value of X rounded to the nearest value $r \cdot i$ with $i \in \mathbb{Z}$. The probability of a measurement $[X]_r$ is equal to probability measuring $Y = [X] + R$, with $|R| < \frac{r}{2}$, where the probability density function of R is uniform on the interval $[-\frac{r}{2}, \frac{r}{2}]$. The probability density function of $[X]_r$ is the convolution of the normal distribution of X and uniform distribution

of R, that is

$$\mathcal{P}(x < [X]_r - X_t) \quad \approx \quad \int_{-\infty}^{[X]_r - X_t} \int_{-\frac{r}{2}}^{\frac{r}{2}} \rho_X(y-s)\rho_R(s)dsdy \tag{B3}$$

$$\Rightarrow \rho_{[X]_r}(y) \quad \approx \quad \int_{-\frac{r}{2}}^{\frac{r}{2}} \rho_X(y-s)\rho_R(s)dsdy = \int_{-\frac{r}{2}}^{\frac{r}{2}} \rho_X(y-s)\frac{1}{r}dsdy \tag{B4}$$

thus the mean and variance of error in $[X]_r$ are

$$\mathcal{P}(x < [X]_r - X_t) \quad = \quad \int_{-\infty}^{[X]_r - X_t} \int_{-\frac{r}{2}}^{\frac{r}{2}} \rho_X(y-s)\rho_R(s)dsdy \tag{B5}$$

$$\Rightarrow \rho_{[X]_r}(y) \quad = \quad \int_{-\frac{r}{2}}^{\frac{r}{2}} \rho_X(y-s)\rho_R(s)dsdy = \int_{-\frac{r}{2}}^{\frac{r}{2}} \rho_X(y-s)\frac{1}{r}dsdy \tag{B6}$$

Appendix C: Data Sources

Table C1 presents the different sources used in the current processing and Figure C1 shows the coverage of the sources processed in 2024/01. Figure C2 shows the number of daily processed observations since 2016. Clearly visible is the sudden decrease in number of ~~observation during the COVID19~~ observations during the COVID-19 period.

Table C1. Sources of Mode-S EHS in the processing dd. 2024/01

source	affiliation	main coverage	ATC/local	first data provided
AS-MET	~~AirSupport, DK~~ Air Support, Denmark	Europe	local receivers	2021-04-15
AU	Austro Control	Austria	ATC radar	2018-09-26
DK	DMI/NAVIAR	Denmark	ATC radar	2017-11-13
ES	~~AEmet~~ AEMET	Spain	ATC radar	2019-06-25
FR	~~MeteoFrance~~ Météo France	France	local receivers	2020-09-08
IL	Israel Meteorological Service	Israel	local receivers	2023-05-01
MUAC	Maastricht Upper ~~Air Control~~ Area Control Centre	Benelux	ATC radar	2014-01
NO-FFI	~~MetNo~~MET Norway/FFI	Norway	local receivers	2021-07-03
RO	ROMATSA	Romania	ATC radar	2020-10-01
SE	SMHI	Sweden	local receivers	2021-06-07
SI	~~SI~~ ARSO	Slovenia	ATC radar	2020-09-08
UK	~~UKMetOffice~~ Met Office	United Kingdom	local receivers	2020-02-01

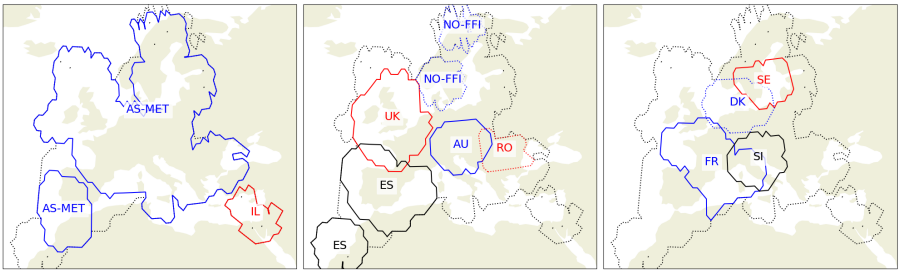

Figure C1. Coverage maps of individual sources: left panel sources AS-MET and IL; middle panel ES, UK, NO-FFI, AU; and right panel : FR, DK, SE and SI.

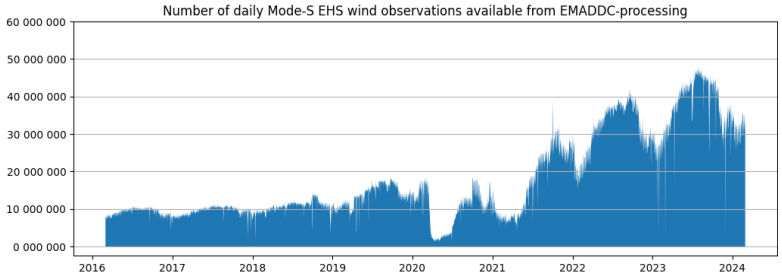

Figure C2. The number of observations per day processed by EMADDC over time.

Author contributions. Siebren de Haan drafted the manuscript and built the first version of EMADDC and the heading correction algorithm and quality control. Siebren de Haan and Paul de Jong further improved the algorithms and quality control. Paul de Jong and Michal Koutek ported the (research) version to an operational system. Jan Sondij is the EMADDC program manager and the liaison between research and the operational aeronautical meteorological service provision and responsible for EMADDC funding and stakeholder management. Lukas Strauss developed the method to improve the Mach number by recalculation using the indicated airspeed. Jan Sondij, Paul de Jong and Michal Koutek provided input for the manuscript draft.

Competing interests. There are no competing interests present.

Acknowledgements. The EMADDC system cannot function without input ~~data in casu~~ Mode-S EHS data. We gratefully acknowledge the delivery of Mode-S EHS data by all our partners for the generation of meteorological information. In particular the provision of Mode-S EHS data by Air Support and the Met Office via a network of local ~~Mode-S/~~ADS-B/Mode-S EHS receivers. Special thanks go out to Torsten Doernbach from EUROCONTROL MUAC who supported the first and important steps with the MUAC data set and provided continuous support. The EMADDC program is co-financed (2016-2024) by the Connecting Europe Facility of the European Union.

References

Barwell, B. R. and Lorenc, A. C.: A Study of the Impact of Aircraft Wind Observations on a Large-Scale Analysis and Numerical Weather Prediction System, Quarterly Journal of the Royal Meteorological Society, 111, 103–129, 1985.

Benjamin, S. G., Jamison, B. D., Moninger, W. R., Sahm, S. R., Schwartz, B. E., and Schlatter, T. W.: Relative Short-Range Forecast Impact from Aircraft, Profiler, Radiosonde, VAD, GPS-PW, METAR and Mesonet Observations via the RUC Hourly Assimilation Cycle, Monthly Weather Review, 138, 1319–1343, 2010.

Cardinali, C., Isaksen, L., and Andersson, E.: Use and Impact of Automated Aircraft Data in a Global 4DVAR Data Assimilation System, Monthly Weather Review, 131, 1865–1877, 2003.

Chulliat, A.: The US/UK World Magnetic Model for 2015-2020, https://doi.org/10.7289/V5TB14V7, 2015.

de Haan, S.: High-Resolution Wind and Temperature Observations from Aircraft Tracked by Mode-S Air Traffic Control Radar, J. Geophys. Res., 116, D10 111–, https://doi.org/10.1029/2010JD015264, 2011.

de Haan, S.: Assimilation of GNSS ZTD and Radar Radial Velocity for the Benefit of Very-Short-Range Regional Weather Forecasts, Q. J. Roy. Met. Soc., https://doi.org/10.1002/qj.2087, 2013.

de Haan, S., de Jong, P. M. A., and van der Meulen, J.: Characterizing and Correcting the Warm Bias Observed in Aircraft Meteorological Data Relay (AMDAR) Temperature Observations, Atmospheric Measurement Techniques, 15, 811–818, https://doi.org/10.5194/amt-15-811-2022, 2022.

Dube, K.: Emerging from the COVID-19 Pandemic: Aviation Recovery, Challenges and Opportunities, Aerospace, 10, 19, https://doi.org/10.3390/aerospace10010019, 2023.

European Commission, .: Commission Implementing Regulation (EU) No 1207/2011 of 22 November 2011 Laying down Requirements for the Performance and the Interoperability of Surveillance for the Single European Sky Text with EEA Relevance, 2011. Superseded by Commission Implementing Regulation (EU) 2023/1770 of 12 September 2023 laying down provisions on aircraft equipment required for the use of the Single European Sky airspace and operating rules related to the use of the Single European Sky airspace and repealing Regulation (EC) No 29/2009 and Implementing Regulations (EU) No 1206/2011, (EU) No 1207/2011 and (EU) No 1079/2012., 2011.

Eyre, J. R.: Observation bias correction schemes in data assimilation systems: a theoretical study of some of their properties, Quarterly Journal of the Royal Meteorological Society, 142, 2284–2291, https://doi.org/https://doi.org/10.1002/qj.2819, 2016.

Ingleby, B., Isaksen, L., and Kral, T.: Evaluation and Impact of Aircraft Humidity Data in ECMWF's NWP System, https://doi.org/10.21957/4e825dtiy, 2020.

Ingleby, B., Candy, B., Eyre, J., Haiden, T., Hill, C., Isaksen, L., Kleist, D., Smith, F., Steinle, P., Taylor, S., Tennant, W., and Tingwell, C.: The Impact of COVID-19 on Weather Forecasts: A Balanced View, Geophysical Research Letters, 48, e2020GL090 699, https://doi.org/10.1029/2020GL090699, 2021.

James, E. P., Benjamin, S. G., and Jamison, B. D.: Commercial-Aircraft-Based Observations for NWP: Global Coverage, Data Impacts, and COVID-19, Journal of Applied Meteorology and Climatology, 59, 1809–1825, https://doi.org/10.1175/JAMC-D-20-0010.1, 2020.

Lange, H. and Janjić, T.: Assimilation of Mode-S EHS Aircraft Observations in COSMO-KENDA, Monthly Weather Review, 144, 1697–1711, https://doi.org/10.1175/MWR-D-15-0112.1, 2016.

Li, Z.: Impact of Assimilating Mode-S EHS Winds in the Met Office's High-Resolution NWP Model, Meteorological Applications, 28, e1989, https://doi.org/10.1002/met.1989, 2021.

Maus, S. and Macmillan, S.: 10th Generation International Geomagnetic Reference Field, Eos Trans. AGU, 86, https://doi.org/10.1029/2005EO160006, 2005.

Mirza, A. K., Ballard, S. P., Dance, S. L., Maisey, P., Rooney, G. G., and Stone, E. K.: Comparison of Aircraft-derived Observations with *in Situ* Research Aircraft Measurements, Quarterly Journal of the Royal Meteorological Society, 142, 2949–2967, https://doi.org/10.1002/qj.2864, 2016.

Painting, J. D.: WMO AMDAR Reference Manual, WMO-No.958, WMO, Geneva, 2003.

Petersen, R. A.: On the Impact and Benefits of AMDAR Observations in Operational Forecasting—Part I: A Review of the Impact of Automated Aircraft Wind and Temperature Reports, Bulletin of the American Meteorological Society, 97, 585–602, https://doi.org/10.1175/BAMS-D-14-00055.1, 2016.

Pourret, V., Mahfouf, J. F., Guidard, V., Moll, O., Doerenbecher, A., and Piguet, B.: Variational bias correction for Mode-S aircraft derived winds, Tellus A: Dynamic Meteorology and Oceanography, 73, 1–27, https://doi.org/10.1080/16000870.2021.1886808, 2021.

Rodi, A. R. and Leon, D. C.: Correction of Static Pressure on a Research Aircraft in Accelerated Flight Using Differential Pressure Measurements, Atmospheric Measurement Techniques, 5, 2569–2579, https://doi.org/10.5194/amt-5-2569-2012, 2012.

Rodriguez, A.: icao.int, https://www.icao.int/NACC/Documents/Meetings/2023/ADSB/ADS-BImp-P07.pdf, [Accessed 27-09-2024], 2023.

Ruijgrok, G. J. J.: Elements of Airplane Performance, Delftse University Pers, 1990.

Schwartz, B. E. and Benjamin, S. G.: A Comparison of Temperature and Wind Measurements from ACARS-Equipped Aircraft and Rawinsondes, Weather and Forecasting, 10, 528–544, https://doi.org/10.1175/1520-0434, 1995.

Stone, E. K. and Kitchen, M.: Introducing an Approach for Extracting Temperature from Aircraft GNSS and Pressure Altitude Reports in ADS-B Messages, Journal of Atmospheric and Oceanic Technology, 32, 736–743, https://doi.org/10.1175/JTECH-D-14-00192.1, 2015.

Stone, E. K. and Pearce, G.: A Network of Mode-S Receivers for Routine Acquisition of Aircraft-Derived Meteorological Data, Journal of Atmospheric and Oceanic Technology, 33, 757–768, https://doi.org/10.1175/JTECH-D-15-0184.1, 2016.

Strajnar, B.: Validation of Mode-S Meteorological Routine Air Report Aircraft Observations, Journal of Geophysical Research: Atmospheres, 117, https://doi.org/10.1029/2012JD018315, 2012.

Strajnar, B., Žagar, N., and Berre, L.: Impact of New Aircraft Observations Mode-S MRAR in a Mesoscale NWP Model, Journal of Geophysical Research: Atmospheres, 120, 3920–3938, https://doi.org/10.1002/2014JD022654, 2015.

Strauss, L.: personal communication, 2017.

Sun, J.: The 1090 Megahertz Riddle: A Guide to Decoding Mode S and ADS-B Signals, TU Delft OPEN Publishing, 2 edn., ISBN 978-94-6366-402-8, https://doi.org/10.34641/mg.11, 2021.

Taylor, J. R.: An Introduction to Error Analysis: The Study of Uncertainties in Physical Measurements, University Science Books, Sausalito, Calif, 2. ed edn., ISBN 978-0-935702-75-0 978-0-935702-42-2, 1997.

WMO: B787 Winds and Other Aircraft Data Quality Issues, https://community.wmo.int/en/activity-areas/aircraft-based-observations/newsletter/volume-22#article-11, [Accessed 27-09-2024], 2022.

WMO: Guide to Instruments and Methods of Observation, vol. Volume III – Observing Systems, ISBN 978-92-63-10008-5, https://library.wmo.int/idurl/4/68661, 2023.

Zhu, Y., Derber, J. C., Purser, R. J., Ballish, B. A., and Whiting, J.: Variational Correction of Aircraft Temperature Bias in the NCEP's GSI Analysis System, Monthly Weather Review, 143, 3774–3803, https://doi.org/10.1175/MWR-D-14-00235.1, 2015.